RADAR CROSS SECTION DEPENDENCE ON WIND SPEED AND WAVE SLOPE

Benjamin E. Barrowes
Brigham Young University, Microwave Earth Remote Sensing (MERS) Laboratory
459 Clyde Building, Provo, UT 84602
801-378-4884, FAX: 801-378-6586, e-mail: barroweb@et.byu.edu

Abstract–YSCAT was an ultrawideband (2-20 GHz), near constant beamwidth scatterometer intended to provide radar cross section (σ_0) measurements at varying radar and environmental parameters. YSCAT was deployed on the CCIW (Canada Centre for Inland Waters) tower on Lake Ontario for a period of six months from June to November, 1994. Using YSCAT data, this paper reports 1) observance of a "low wind-speed cut-off", the fall-off of σ_0 which occurs at low wind speeds, and 2) the results of fitting a Rayleigh/2-component log-normal probability distribution to the observed backscattered power measurements at C-band (5 GHz) and X-band (10 GHz). The observed characteristic trends of the fitted pdf model parameters verses wind speed and wave slope are shown. and discussed.

Introduction

The air-sea interface is a complex, constantly changing boundary layer between the atmosphere and Earth's oceans. Much research has been devoted to understanding this interface and the role it plays in global weather and in the natural environment. In spite of this research, our understanding of the mechanisms involved at this interface remains poor.

The relationship between the wind and the waves generated on the sea surface is of primary importance. As the wind speed over the water increases, first small capillary waves, then longer wavelength waves are generated. Eventually a wave spectrum emerges, and the wind and waves reach a steady state called a fully developed sea. The process through which this generation occurs, including when and what wavelength of waves are generated by a given wind speed, is still debated.

Radar scatterometry has been an effective tool used to increase our understanding of the air sea interface since the 1960's with one of the main objectives being satellite anemometry. In order to more fully understand the data collected by spaceborne scatterometers such as NSCAT, ERS-1, and the soon to be launched QuikSCAT, tower mounted scatterometers such as YSCAT provide a cost effective way to study the air sea interface.

YSCAT was developed to study the air-sea interface under varying radar and environmental parameters [Collyer, 1994]. In one of its operational modes, YSCAT collected data at five principal frequencies of 2, 3.05, 5.3, 10.02, and 14 GHz, eight incidence angles of 0° (nadir), 10°, 20°, 25°, 30°, 40°, 50°, and 60°, and at both horizontal and vertical polarizations. In this mode the azimuth angle of YSCAT was adjusted to track the wind direction, with both upwind and downwind measurements obtained. In this paper, "upwind" and "downwind" include 20° on either side of the true wind direction. Sorting the recorded data according to wind speed and mean square wave slope, 3200 distinct cases of the previous parameters emerge on which to draw conclusions which may increase understanding of the air-sea interface.

Analysis of each of the 3200 cases separately would be impractical in this setting; instead, an analysis of a few cases at wind speeds of 1-10 m/s and wave slopes of 0.1-0.8 are presented. Results will be summarized and compared to other cases and the implications discussed.

Low Wind Speed Rolloff

Donelan and Pierson [Donelan and Pierson, 1987] postulated the existence of a roll off of σ_0 versus wind speed. At very low wind speeds, the friction velocity is too small to generate small waves, resulting in a smooth surface and a small backscatter cross section. At higher wind speeds, the wind generates capillary waves and σ_0 closely follows a power-law relationship with wind speed. This effect has been observed in carefully controlled wave tank data where a hysteresis effect in σ_0 versus wind speed is observed [Plant et al., 1999a]: as the wind speed is increased from zero, at a temperature-dependent threshold wave generation commences and σ_0 increases significantly. As the wind speed is decreased, waves are maintained at wind speeds below the startup threshold and finally fall off. The thresholds at which wave generation begins and ends is very temperature and long wave field sensitive.

While this effect has been observed in wave tank data [Plant et al., 1999a] and in airship scatterometer data [Plant et al., 1999b], it has not previously been reported in tower data. However, YSCAT data provides strong evidence to support this low wind speed roll off over a wide range of frequencies. For example, Fig. 1 illustrates a typical plot of YSCAT σ_0 measurements versus wind speed. This example is for 3 GHz at 20° incidence angle and is typical of YSCAT data. We note that there is a dramatic rolloff in the received power at wind speeds less than about 4 m/s. The broad wind speed spread in the falloff region supports the hysteresis effect observed

in wave tank data since there is a range of long wave and temperature conditions as well as wind fluctuations in the uncontrolled environment of the tower experiment. We postulate that the fall off has not been observed in space borne scatterometer measurements due to wind variability over the large area footprints of such instruments. Over the range of frequencies and incidence angles observed by YSCAT, the fall off threshold varies from 3 to 6 m/s.

2-Component Log-normal/Rayleigh Distribution

Thompson and Gotwols [Gotwols and Thompson, 1994] proposed a probability distribution for modeling microwave radar backscatter based on conditional probabilities,

$$p(a) = \int_0^\infty p(a|\sigma_\circ)p(\sigma_\circ)d\sigma_\circ. \qquad (1)$$

This model for radar backscatter from water waves assumes that the wave spectrum consists of two scales of waves: waves smaller than the dominant wave length but on the order of the scatterometer footprint or smaller, and dominant wavelength waves larger than the scatterometer footprint. On scales shorter than the longer dominant waves, $\sigma_\circ$ is assumed to be constant with amplitude a being described by a conditional probability $p(a|\sigma_\circ)$. For longer wavelengths, $\sigma_\circ$ is allowed to vary yielding the probability $p(\sigma_\circ)$. If both $p(a|\sigma_\circ)$ and $p(\sigma_\circ)$ were known, the backscatter amplitude probability distribution $p(a)$ could be calculated using Eq. 1.

The distribution of $p(a|\sigma_\circ)$ has been debated, with Thompson and Gotwols [Gotwols and Thompson, 1994]

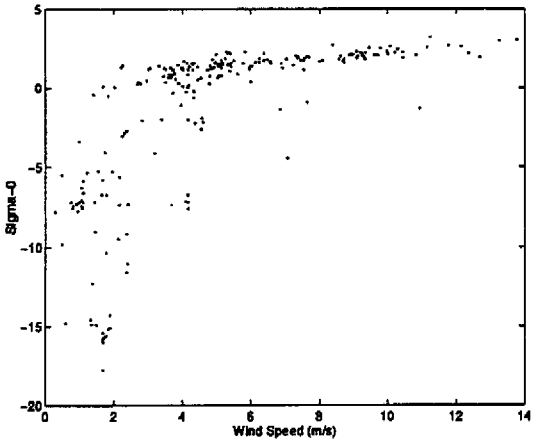

Figure 1: Typical YSCAT backscatter response illustrating the low wind speed roll off of $\sigma_\circ$. Data is for 3 GHz, vertical polarization, upwind, 20° incidence angle.

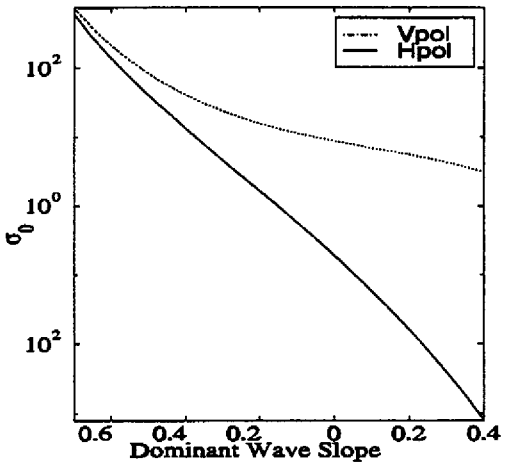

Figure 2: Dominant wave slope versus $\sigma_\circ$ plotted from the Donelan spectrum [Donelan et al., 1985]. 14 GHz, wind speed 8m/s, fetch is 9km.

concluding that for their data, $p(a|\sigma_\circ)$ was Rayleigh distributed. YSCAT's backscatter sampling frequency of 10 Hz is too low (compared to the 1-3 KHz sampling rate of [Gotwols and Thompson, 1994]) to test its data by removing the underlying $p(\sigma_\circ)$ dependence. The present analysis assumes that $p(a|\sigma_\circ)$ is indeed Rayleigh distributed.

The distribution of $p(\sigma_\circ)$ can be derived by starting at the theoretical result for $\sigma_\circ$ given by small perturbation theory [Gotwols and Thompson, 1994]

$$\sigma_\circ = 16\pi k_m^4 |g_{ii}(\theta_i)|^2 \Psi(2k_m \sin\theta_i, 0). \qquad (2)$$

where $\sigma_\circ$ is the radar cross section, θ_i is the incidence angle, $g_{ii}(\theta_i)$ is a polarization dependent reflection coefficient with ii being hh or vv, k_m is the microwave wavenumber ($\omega\sqrt{\mu\epsilon}$ or $\frac{2\pi}{\lambda}$), and Ψ is the wave height spectral density [Reed, 1995].

The wave height spectral density (Ψ) is assumed to be a Donelan spectrum since it was developed by Donelan using wave staff data taken at the same site where YSCAT was deployed. For a detailed description of the Donelan Spectrum, see [Donelan et al., 1985]. The reflection coefficients $g_{ii}(\theta_i)$ may be written as [Donelan et al., 1985]

$$|g_{vv}(\theta_i)|^2 = \frac{\cos^4\theta_i(1+\sin^2\theta_i)^2}{(\cos\theta_i + 0.111)^4} \qquad (3)$$

and

$$|g_{hh}(\theta_i)|^2 = \frac{\cos^4\theta_i}{(0.111\cos\theta_i + 1)^4} \qquad (4)$$

where θ_i is the incidence angle between the radar and the water surface.

Using the definitions

$$\chi + \theta_i = \theta_o \tag{5}$$

and

$$\tan \chi = -s_x. \tag{6}$$

where θ_i is the local incidence angle, θ_o is the nominal incidence angle, and s_x is the wave slope (see Fig. 3) and

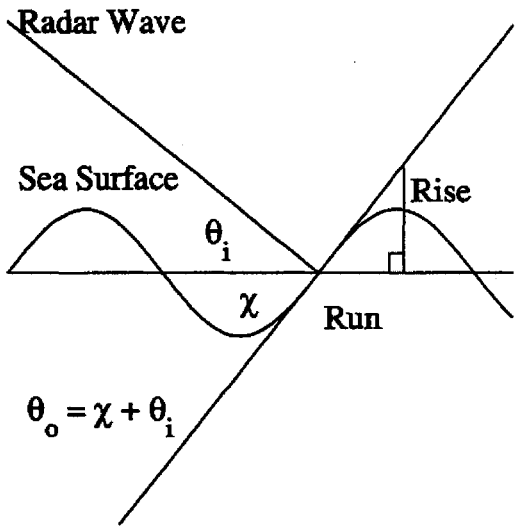

Figure 3: Relationship between χ, θ_i, and θ_0. Wave slope s_x can be described by the "rise" over the "run".

writing $p(\sigma_o)$ in terms of s_x using the transformation law

$$p(\sigma_o) = \frac{p(s_x)}{|d\sigma_o/ds_x|} \tag{7}$$

yields the relationship between s_x and σ_o illustrated in Fig. 2. The shape of these curves for mid-range incidence angles can be reasonably approximated by a first or second order fit in log space [Gotwols and Thompson, 1994]. Thus, in general, σ_{op} may be expressed as a two component exponential

$$\sigma_{op} = Ce^{a_1 s_x + a_2 s_x^2} \tag{8}$$

where p is either v or h. $p(\sigma_{op})$ may be expressed using Eq. 7 as [Gotwols and Thompson, 1994]:

$$p(\sigma_{oh}) = \frac{1}{a_1 \sigma_x \sigma_{oh} \sqrt{2\pi}} \exp\left\{ \frac{-(ln\sigma_{oh} - lnC)^2}{2a_1^2 \sigma_x^2} \right\} \tag{9}$$

for horizontal polarization (a_2=0), and

$$p(\sigma_{ov}) = \frac{1}{(a_1 + 2a_2 s_x)\sigma_x \sigma_{ov} \sqrt{2\pi}} \exp\left\{ \frac{-(s_x)^2}{2\sigma_x^2} \right\} \tag{10}$$

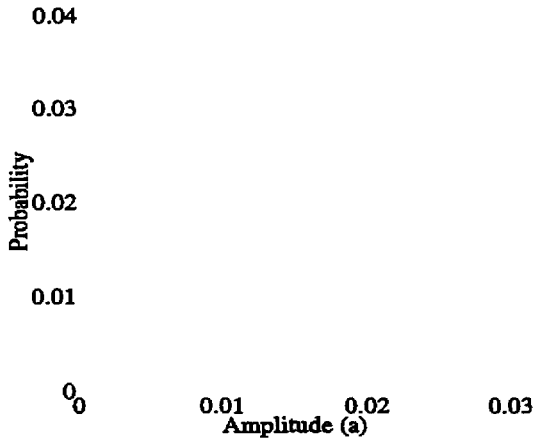

Figure 4: Weibull and Rayleigh/2-component log-normal distributions fitted to YSCAT data. Weibull distribution shown as dashed line. The Rayleigh/2-component log-normal distribution is obscured by the data due to the excellent fit. Data is for 5 GHz, v-pol, downwind, 20°, 2 m/s wind speed case. Rayleigh/2-component log-normal parameters are a_1=17.57, a_2=-5.58, σ_x=0.0914, and C=5.85e4.

for vertical polarization ($a_1, a_2 \neq 0$), with s_x defined by Eq. 8 assuming $p(s_x)$ is normally distributed with 0 mean.

Equation 9 is the common log-normal probability distribution whose mean and variance are given by

$$\begin{aligned} \mu_{1n} &= \lim_{a \to \infty} \int_0^a \frac{1}{\sigma_x a_1 \sqrt{2\pi}} \exp\left\{ -\frac{(\ln \frac{\sigma_h^o}{C})^2}{2a_1^2 \sigma_x^2} \right\} d\sigma_h^o \\ &= \lim_{a \to \infty} -\frac{1}{2} C e^{\frac{\sigma_x^2 a_1^2}{2}} \operatorname{erf}\left\{ \frac{\sigma_x^2 a_1^2 - \ln \frac{\sigma_N^2}{C}}{\sigma_x a_1 \sqrt{2}} \right\} \Bigg|_{\sigma_N^2 = 0}^{\sigma_N^2 = a} \\ &= Ce^{\frac{\sigma_x^2 a_1^2}{2}} \end{aligned} \tag{11}$$

and the variance is

$$\begin{aligned} \sigma_{1n} &= \lim_{a \to \infty} \int_0^a \frac{\sigma_h^o}{\sigma_x a_1 \sqrt{2\pi}} \exp\left\{ -\frac{(\ln \frac{\sigma_h^o}{C})^2}{2a_1^2 \sigma_x^2} \right\} d\sigma_h^o \\ &= C^2 (e^{2\sigma_x^2 a_1^2} - e^{\sigma_x^2 a_1^2}). \end{aligned} \tag{12}$$

Equation 10 has no commonly accepted name, but will be referred to as the 2-component log-normal probability distribution. The mean and variance of the 2-component log-normal distribution are

$$\mu_{2ln} = \frac{C \exp\left(\frac{a_1^2 \sigma_x^2}{1 - 2a_2 \sigma_x^2}\right)}{\sqrt{1 - 2a_2 \sigma_x^2}}. \tag{13}$$

and

$$\sigma_{2ln} = \frac{C^2 \exp\left(\frac{2a_1^2\sigma_x^2}{1-4a_2\sigma_x^2}\right)}{\sqrt{1-4a_2\sigma_x^2}}. \quad (14)$$

Equations 11, 12, 13, and 14 are helpful when "guessing" seed values for the optimization routine (see below).

Fitting the Distribution

Knowing functional forms for both $p(a|\sigma_a)$ (Rayleigh distributed) and $p(\sigma_a)$ (2-component log-normal distributed), and again using Eq. 7, Eq. 1 may be written as:

$$p(a) = \int_{-\infty}^{\infty} \underbrace{\frac{e^{a_1 s_x + a_2 s_x^2} e^{-a^2 C e^{a_1 s_x + a_2 s_x^2}}}{(2aC)^{-1}}}_{p(a|\sigma_a(s_x))} \underbrace{\frac{e^{\frac{-s_x^2}{2\sigma_x^2}}}{\sqrt{2\pi}\sigma_x}}_{p(\sigma_x(s_x))} ds_x. \quad (15)$$

Note that the integration limits have been adjusted due to the change of variables from σ_0 to s_x.

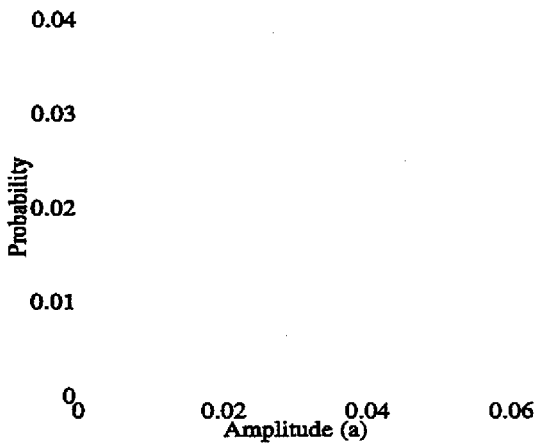

Figure 5: Backscatter distributions for 5 GHz, v-pol, downwind, 20°, 2 and 6 m/s. Lower curve is for 2 m/s. Parameters for 6 m/s case are a_1=19.2, a_2=-14.8, σ_x=0.0914, and C=2.14e4.

The analytical solution to Eq. 15 has not been found by the authors. However, this integral may successfully be evaluated numerically. For any given values of a_1, a_2, σ_x, and C, this integral can be numerically approximated for any value of a. When tabulated for a sufficient number of a's, a distribution emerges. This distribution can then be fit to data using the Gauss-Newton minimization technique. An example is given in Fig. 4 for the case of 5 GHz, v-pol, downwind, 20°, and 2 m/s.

In the majority of cases, the Rayleigh/2-component log-normal distribution fits YSCAT data extremely well. Distributions were fit to YSCAT data by minimizing the

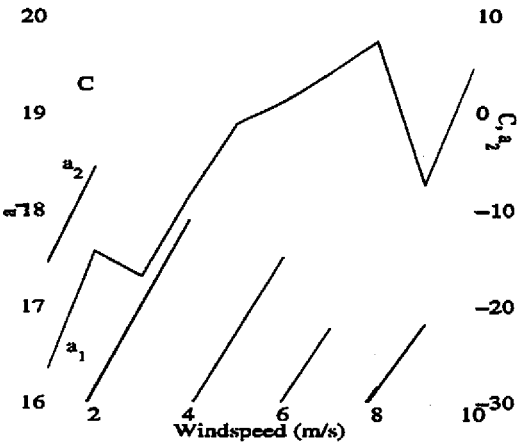

Figure 6: a_1, a_2, and C values for 5 GHz, v-pol, downwind, 20°, 1-10 m/s. C values are scaled by the relation $20log_{10}(|C|) - 100$.

Kullback-Leibler distance [Cover and Thomas, 1990], which provides a measure of the "distance" between two discrete distributions and is given by

$$p(f||g) = \sum_{n=-\infty}^{\infty} \left| f(x_n) \log \frac{f(x_n)}{g(x_n)} \right|. \quad (16)$$

All of the YSCAT data has been parameterized with the Rayleigh/2-omponent log-normal distribution. Care must be taken, however, because in four variables, a_1, a_2, σ_x, and C, Eq. 15 is degenerate (*i.e.* it has non-unique solutions). However, σ_x may be calculated from *in situ* wave staff measurements. Choosing σ_x guarantees a unique solution (except in a_1, see below). For simplicity, all cases presented in this paper use σ_x = 0.0914. Equation 15 is also symmetric with respect to the sign of a_1 (*i.e.*, a_1 and $-a_1$ yield the same distribution) as may be suspected by noting that the mean and variance (Eqs. 13, and 14) are also symmetric with respect to the sign of a_1. For this reason, plots of the parameter a_1 plot the absolute value of a_1. One example of the fitted distribution is shown in Fig. 4, another in Fig. 5 with the previous distribution included for reference.

The two distributions are significantly different with the 6 m/s case having a much longer tail and greater mean. This difference is reflected in the fitted parameters with increasing a_1 and decreasing a_2 and C. This is a common trend in YSCAT data. Figures 6 and 7 show parameter values for data at 5 and 10 GHz respectively.

Mean Squared Wave Slope

YSCAT data was also binned according to the mean square wave slope. The mean square wave

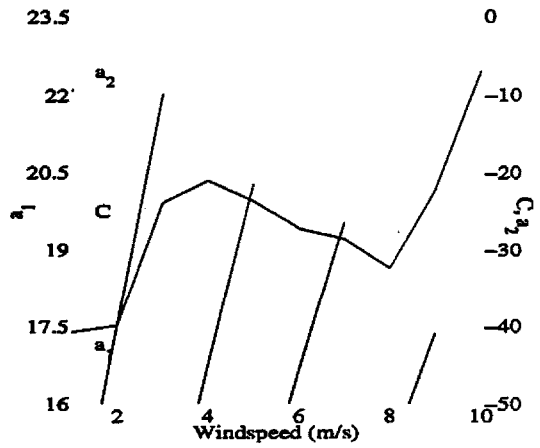

Figure 7: a_1, a_2, and C values for 10 GHz, v-pol, downwind, 20°, 1-10 m/s. C values are scaled by the relation $10log_{10}(C) - 100$.

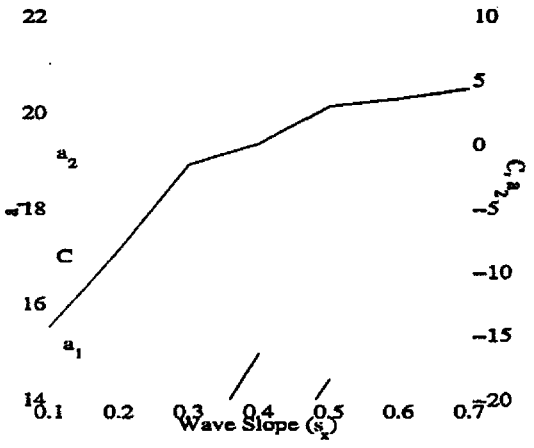

Figure 8: a_1, a_2, and C values for 5 GHz, v-pol, downwind, 20°, 0.1-0.7 wave slope. C values are scaled by the relation $20log_{10}(C) - 100$.

slope can be calculated from radar data alone [Melville and Felizardo, 1999] [Smith, 1999], but an array of wire wave staves was installed on the CCIW tower during YSCAT's deployment period. Using these wave staff measurements, the mean square wave slope (s_x) may be calculated using a method described by Cox and Munk [Cox and Munk, 1956]. First the surface height spectrum is computed from the 10 Hz sampled wave staff measurements. Then, the slopes spectrum is calculated by

$$S(f_i) = \frac{(2\pi f_i)^4}{g^2}\Phi(f_i) \qquad (17)$$

where f_i is the frequency, $S(f_i)$ is the slope spectrum, g is the gravitational acceleration constant, and $\Phi(f_i)$ is the surface height spectrum. Last, the mean square wave slope estimate s_x is calculated using the relation

$$s_x = \left[\frac{1}{N - M + 1}\sum_{i=M}^{N}\frac{(2\pi f_i)^4}{g^2}\Phi(f_i)\right]^{\frac{1}{2}} \qquad (18)$$

where N is the frequency bin corresponding to the upper cutoff, and M is the frequency bin corresponding to the lower cutoff [Barrowes, 1999].

s_x estimates ranged from 0-0.8 with 0.1-0.8 taken to be valid data. The 2-component log-normal distribution parameters a_1, a_2, and C were tabulated for the same data cases as Figs. 6 and 7 according to wave slope instead of wind speed and are presented in Figs. 8 and 9 respectively.

Discussion

Backscatter distributions from YSCAT at 5 and 10 GHz, v-pol, downwind, 20° incidence angle, for 1-10 m/s wind

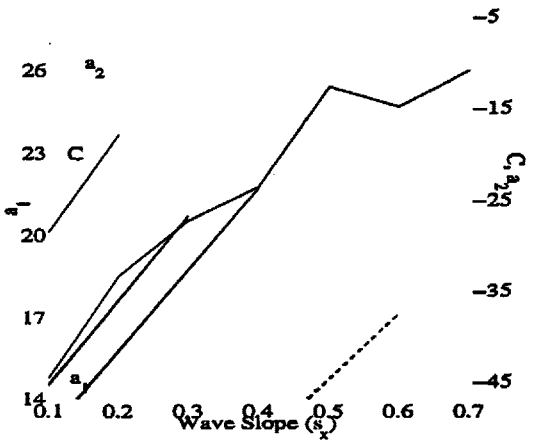

Figure 9: a_1, a_2, and C values for 10 GHz, v-pol, downwind, 20°, 0.1-0.7 wave slope. C values are scaled by the relation $10log_{10}(C) - 100$.

speeds and 0.1-0.8 mean square wave slopes were shown to exhibit characteristic trends when parameterized by a combined Rayleigh/2-component log-normal distribution. These trends could prove useful in increasing our understanding of the effect of environmental parameters on radar backscatter.

REFERENCES

[Barrowes, 1999] Barrowes, B. E., *YSCAT Backscatter Distributions*. Master's thesis, Brigham Young University, 1999.

[Collyer, 1994] Collyer, R. S., *Wind Speed Dependence of the Normalized Radar Cross Section*. Master's the-

sis, Brigham Young University, Provo, UT, 1994.

[Cover and Thomas, 1990] Cover, T. M. and J. M. Thomas, *Elements of Information Theory*. New York: Wiley, 1990.

[Cox and Munk, 1956] Cox, C. and W. H. Munk, "Slopes of the Sea Surface Deduced from Photographs of Sun Glitter." *Bulletin of the Scripps Institute of Oceanography of the University of California*, vol. 6, no. 9, pp. 401–488, 1956.

[Donelan et al., 1985] Donelan, M. A., J. Hamilton, and W. H. Hui, "Directional Spectra of Wind-Generated Waves." *Philosophical Transactions of the Royal Society of London*, vol. 315, no. A, pp. 509–562, 1985.

[Donelan and Pierson, 1987] Donelan, M. A. and W. J. Pierson, "Radar Scattering and Equilibrium Ranges in Wind Generated Waves with Application to Scatterometry." *IEEE Journal of Geoscience and Remote Sensing*, vol. 92, no. C5, pp. 4971–5029, 1987.

[Gotwols and Thompson, 1994] Gotwols, B. L. and D. R. Thompson, "Ocean Microwave Backscatter Distributions." *Journal of Geophysical Research*, vol. c5, no. 99, pp. 9741–9750, 1994.

[Melville and Felizardo, 1999] Melville, W. K. and F. C. Felizardo, "The Influence of Wave Slope and Elevation on EM Bias." Author provided a rough draft.

[Plant et al., 1999a] Plant, W. J., W. C. Keller, and D. E. W. M. A. Donelan, "A Wind Speed Threshold in Microwave Scattering from the Ocean." URSI Meeting, Boulder, CO, 1999a.

[Plant et al., 1999b] Plant, W. J., D. Weissman, W. Keller, V. Hesany, K. Hayes, , and K. Hoppel, "Air/sea momentum transfer and the microwave cross section of the sea." *Journal of Geophysical Research*, 1999b.

[Reed, 1995] Reed, R., *Statistical Properties of the Sea Scattered Radar Return*. Dissertation, Brigham Young University, 1995.

[Smith, 1999] Smith, J. D., *Studies to Improve the Estimation of the Electromagnetic Bias in Radar Altimitry*. Master's thesis, Brigham Young University, 1999.